ANALYSIS OF THE DIFFERENTIAL-GROWTH METHOD'S POTENTIAL FOR DESIGNING COMPLEX HEAT-TRANSFERRING WALLS FOR COMPACT HEAT EXCHANGER

Seidler, Alexander;
Holtzhausen, Stefan;
Sander, Maximilian;
Paetzold-Byhain, Kristin

Technische Universität Dresden

ABSTRACT

Water scarcity and resource depletion can be expected during the climate crisis. Therefore, thermally loaded processes in particular, must be made more efficient in the future. Heat exchangers will play a key role in this optimization process. More efficient designs allow a greater heat flow to be removed from processes while mass flows remain constant. In this context, the heat-transferring wall of heat exchangers is a focus of current research on the design of heat exchangers. The aim is to increase the heat-transferring surface of the wall as much as possible and to keep the design space as compact as possible. Therefore, this study investigates the suitability of the differential-growth method for generating complex heat-transferring walls for heat exchangers using CFD-analysis. Firstly, a framework for generating the wall structures and a computational model for predicting the design influence of such structures for the thermal and fluid-dynamic behavior of the heat exchanger are presented. Thereby, the potential of such wall structures is analyzed in this study. Furthermore, the study identified weaknesses of such walls designed with the differential-growth method, which should be the focus of future investigations.

Keywords: Computational design methods, Design for Additive Manufacturing (DfAM), Simulation

Contact:
Seidler, Alexander
Technische Universität Dresden
Germany
alexander.seidler@tu-dresden.de

Cite this article: Seidler, A., Holtzhausen, S., Sander, M., Paetzold-Byhain, K. (2023) 'Analysis of the Differential-Growth Method's Potential for Designing Complex Heat-Transferring Walls for Compact Heat Exchanger', in *Proceedings of the International Conference on Engineering Design (ICED23),* Bordeaux, France, 24-28 July 2023. DOI:10.1017/pds.2023.59

1 INTRODUCTION

Water scarcity and resource depletion can be expected during the climate crisis. Therefore, thermally polluted processes in particular, must be designed more efficiently in the future. Heat exchangers will play a key role in this optimization process. More efficient designs allow a greater heat flow to be dissipated from the processes while maintaining similar mass flows. As a result, less material is needed to manufacture these components and less cooling fluid is required in the process. The importance of heat exchangers for the climate-friendly design of technical processes was already addressed by Shah et al. (2000). Heat exchangers remove or supply energy from or to a system during this process. The exchange of thermal energy is achievable in different ways. For this purpose, the use of heat exchangers in the technology sector is more likely. Therefore, they are designed to separate the thermally relevant fluids by one or more separating walls. As a result, the heat is transferred indirectly between the fluids.

For this reason, all optimization approaches in this field aim to increase the heat-transferring surface of the fluid-separating wall and reduce its thickness (Peng *et al.*, 2019). However, this should be realized in the smallest possible space to increase the energy exchange between the different fluids. In addition, the thermal load on the heat-transferring partition wall also poses a challenge. Materials with a high thermal load capacity often show poor thermal conductivity properties while being high-cost, which results in further economically and thermally motivated requirements for the design (Peng *et al.*, 2019).

In this context, the research benefits significantly from the successes achieved in additive manufacturing, particularly metallic 3D printing, which means that nearly no manufacturing restrictions are imposed on designing new and complex wall structures (Jafari and Wits, 2018).

Especially in the last ten years, heat exchanger design research has focused on periodic minimal surface models approximating triply periodic minimal surface (TPMS) models (Peng et al., 2019; Attarzadeh *et al.*, 2021; Attarzadeh *et al.*, 2022; Li *et al.*, 2020;). Due to their high porosity, these designs have a high surface area and can be manufactured without support structures and with low wall thicknesses using additive manufacturing. In several investigations, this heat exchanger's flow ability and suitability have already been examined (Peng *et al.*, 2019; Attarzadeh *et al.*, 2021; Attarzadeh *et al.*, 2022; Li et al., 2020; Zhu *et al.*, 2021). However, several studies have already shown that, in addition to good heat transfer, these structures exhibit an exponential increase in pressure drop as flow velocities increase. (Peng *et al.*, 2019; Li *et al.*, 2020; Attarzadeh *et al.*, 2021; Attarzadeh *et al.*, 2022; Genç *et al.*, 2022). One reason for this is the higher surface area which leads to greater frictional influences on the flow pattern. Another is the complex geometric design leading to a turbulent behavior of the fluids and favors heat transfer while increasing the pressure drop because of undesirable and bad controllable fluid behavior. Furthermore, the supply of fluids with parallel or countercurrent principles is complicated since the inflow profile design for such structures is associated with an increased design effort, which is why realizations of these designs have so far only been solved via cross-flow principles (Peng et al., 2019; Vlahinos and O'Hara, 2020). It has already been confirmed in initial experimental investigations that the pressure drop of these structures is very strongly dependent on the flow velocity, which means that their use in heat exchangers involves considerable pumping power and regulates their applicability for technical processes. (Genç *et al.*, 2022).

Of course, other approaches and algorithms also offer the potential for generating complex wall structures with large heat transfer surfaces. For example, digital art and geometric mathematics use algorithms for generating space-filling curves, according to Gotsman and Lindenbaum (1996) and Pedersen and Singh (2006). Based on these curves, complex wall structures with high heat-transferring surfaces could subsequently be developed. Yet, fractal geometries, according to Gotsman and Lindenbaum (1996), are geometrical shapes based on similar geometrical parts. However, such geometries are challenging to design and manufacture because small wall thicknesses are needed, which is still challenging for additive manufacturing. In addition, such structures cannot be approximated on every cross-section. In contrast, the approach to generate space-filling curves, the differential-growth method, according to Pedersen and Singh (2006) based on Gotsman and Lindenbaum (1996), is promising since the resulting structures are adaptable to any cross-section. Moreover, with these structures' growing properties, local design behavior based on flow patterns and temperature distribution will be conceivable soon. Therefore, the differential-growth method is promising for designing and analyzing suitable wall structures for heat transfer.

https://doi.org/10.1017/pds.2023.59 Published online by Cambridge University Press

To the authors' knowledge, this method has yet to be investigated in any technical publication under the aspects mentioned here. The software company *Hyperganics* has already published one of the first geometry results in designing nozzles, indicating the differential-growth method's use. However, there is no data basis for the geometry generation. Furthermore, numerical investigations of such structures have yet to be discovered, and neither is there any assessment of the potential of the differential-growth method for generating heat-transferring walls in heat exchangers.
Therefore, this study will use the differential-growth method to present a framework for CAD-enabled geometry generation of complex wall structures for heat exchangers. Based on the presented structures, the potential of this method for generating complex wall structures compared to TPMS structures will be investigated using numerical investigations (CFD) to contribute new approaches to the complex design of technically relevant structures in this field of research.

2 MATERIAL AND METHODS

2.1 Algorithmic geometry design

In order to generate wall structures with the differential-growth method, a space-separating start curve is specified in the design area. Next, the start curve is discretized over a defined number of support points. Based on the position of each point, the attractive and repulsive forces to all surrounding points are calculated (Figure 1 left). The dominant forces are proportional to the distance between the points and scaled by a fictitious velocity parameter. Subsequently, all forces acting on each point of the curve are averaged. Afterwards, each point is moved along its averaged force vectors and the length of the curve increases. When moving the points, an additional check is made to see if the new position of the points is in the design space, otherwise, no move is made.
Furthermore, support points are inserted on the curve if the distance between two neighboring points is too large. Thus, more aggressive convolutions can be induced. On this basis, the geometry generation method was adapted to the requirements of generating wall structures. Thereby, one parameter each is defined for the wall thickness (t_w) and for the minimum width (t_f) between the furrow-forming walls of the structure. Thus, the collision of approaching walls can be avoided (Figure 1 right). Likewise, these parameters are used to calculate the collision distance (t_c) (1) and the minimum distance of the walls to the design space (t_b) (2). Based on these parameters, it is ensured that the generated furrow guarantees an approach and a throughflow, respectively.

$$t_c = t_w + t_f \tag{1}$$

$$t_b = 0.7 * (t_w + t_f) \tag{2}$$

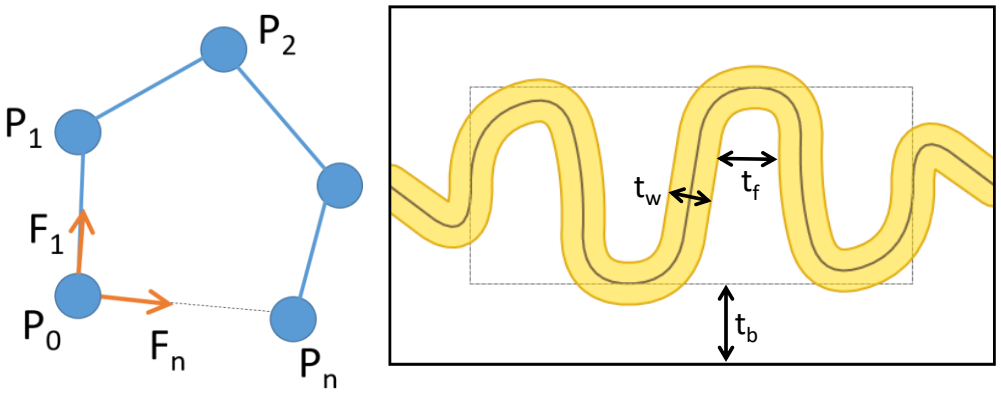

Figure 1. Visual representation of the implemented differential-growth method

The furrows of the wall are getting generated via an iterative process. The change in the curve length between each iteration is the termination criterion for the curve generation. Thus, the geometry generation is aborted when the curve's length no longer changes by a specified threshold value (Figure 2). In the case of binary spatial separation, a furrow balance is always achieved for both fluids. The fluids shown in the figure are a cold fluid (blue), a hot fluid (red) and a heat-transferring wall (gray).

https://doi.org/10.1017/pds.2023.59 Published online by Cambridge University Press

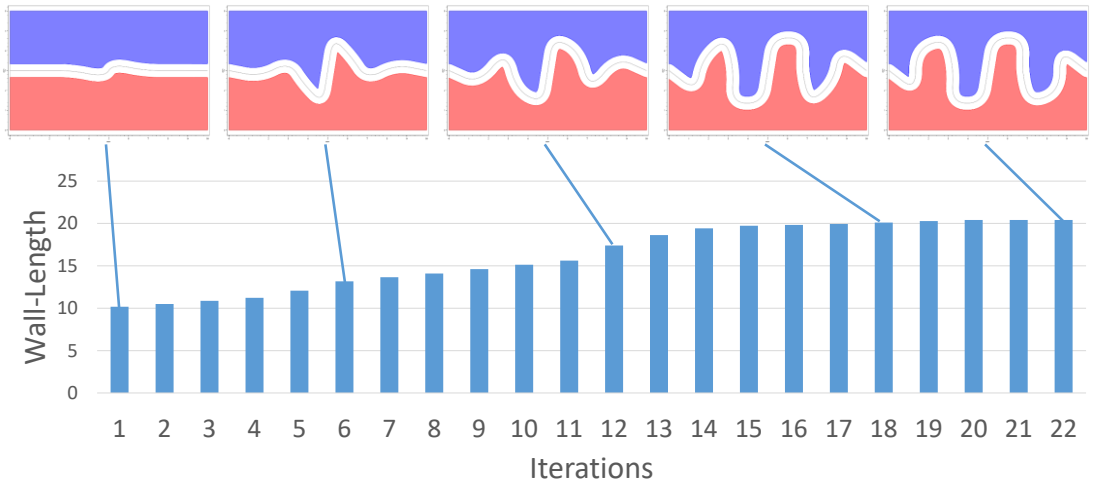

Figure 2. Growing the wall design (gray) with the iterative reaching of the convergence of the hot fluid region (red) and the cold fluid region (blue).

Afterward, the curves get saved layer by layer in the .dxf-file format as an interface format to *Ansys SpaceClaim*. A defined offset value shifts the curves' sketching plane (X-Y plane) in the Z-direction (Figure 3 right). Subsequently, the loft function merges the generated curves to a surface (Figure 3). Afterward, the surface is thickened by the offset (t_w). Next, the offset surface is merged with the original lofted curve surface to form a solid wall. Due to the curves' iterative generation, these structures' inflow area can be generated without much design effort (Figure 3).

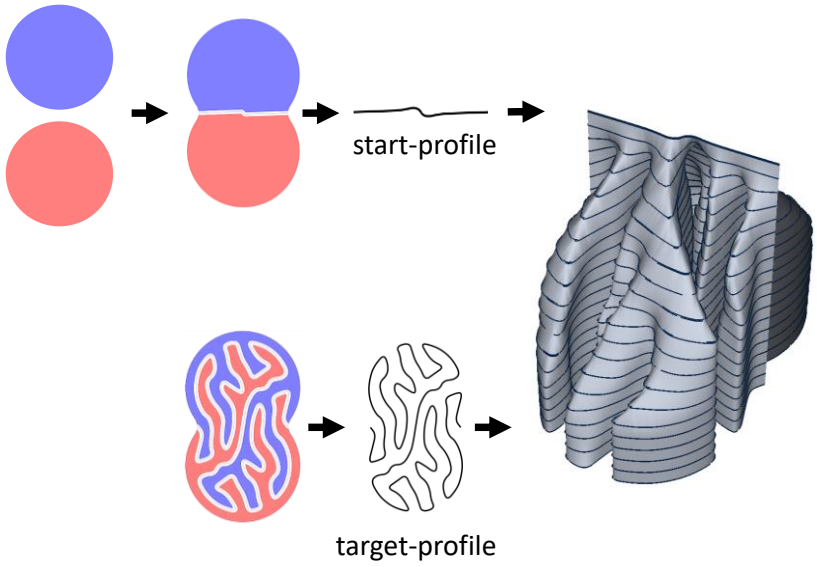

Figure 3. Principal framework for generating geometry models

At this point, wall structures for various cross-sections can be realized easily with this method. Wall structures were generated for different shell geometries to prove the design freedom (Figure 4 left). For example, in addition to complex shell geometries, complex hole geometries were also defined to be excluded from the wall generation (Figure 4 right).

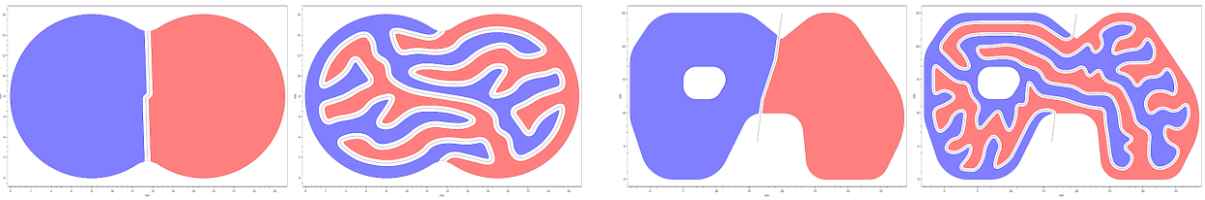

Figure 4. The freedom of designing wall structures created with the investigated differential-growth method by the example of complex cross-sections

https://doi.org/10.1017/pds.2023.59 Published online by Cambridge University Press

Based on this method (Figure 2) a geometry for a cross-sectional area with a width of 40 mm and a height of 20 mm was generated (Figure 5). These dimensions were taken from the study published by Peng et al. (2019) to establish the comparability of the wall structure presented in this paper with a heat exchanger based on a gyroid wall structure. In this study, the length of the heat exchanger is 100 mm and generated by the loft function (Figure 3). The inflow and outflow areas of the structures were not considered in this study in order to investigate the fully formed cross-sectional structure. The developed cross-section of the developed heat exchanger (gray) generated by the presented method (Figure 2) is shown with the hot fluid (red) and the cold fluid (blue) (Figure 5). Due to manufacturing constraints, the wall thickness was set to 0.7 mm rather than 0.5 mm (Peng *et al.*, 2019) to allow experimental validation in the future. The surface area of the heat-transferring wall of the heat exchanger is 40460 mm² (0.040 m²). The cross-sectional area of the fluid regions is 252.2 mm² each.

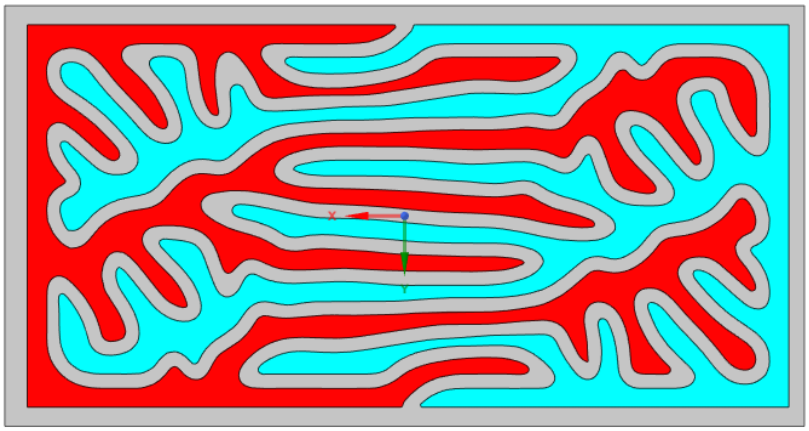

Figure 5: Cross-section of the designed heat-transferring wall (gray) of the analyzing heat exchanger with the hot fluid (red), and the cold fluid (blue)

2.2 Numerical investigation setup

2.2.1 Boundary conditions

To evaluate the generated wall structures and ensure comparability with other approaches, a first assessment of the generated heat-transferring wall will be performed using computational fluid dynamic simulations (CFD) with the software *Ansys® Academic Research Fluent 2021 R2*. The structure will be analyzed for its flow and heat transfer properties. For comparability reasons, the calculation model's structure will be based on Peng et al. (2019). This section gives all information on physical quantities in SI units for simplified comprehensibility and replication of the model.

Peng et al. (2019) used simplified calculation approaches for calculating and evaluating their investigated TPMS-approximated wall structure in the software *COMSOL*. These assumptions are primarily adopted in this calculation model presented here, too. The simplifications made here are used exclusively for estimating potential and not for the technical design of the heat exchangers. This study investigates the heat transport of a hot fluid (373.15 K) and a cold fluid (293.15 K) at a velocity of 0.02 m/s. The fluids are incompressible liquid water. The material of the heat exchanger is copper. The defined material models are listed in Table 1. A constant pressure of 0 Pa is defined at the flow outlet. The walls of the heat exchanger are defined as stationary with a no-slip shear condition and a frictionless wall boundary. The fluid-solid interface is coupled to the thermal conditions (Baker, 2021). Since the structure studied here is also a thin wall, a simplified wall thickness of 0 m is assumed (Peng *et al.*, 2019).

Table 1: Material properties

Material	Density ρ [kg/m³]	Dynamic viscosity η [kg/(m*s)]	Specific heat capacity c_p [J/(kg*K)]	Thermal conductivity K [W/(m*K)]
Water (20°C)	998.00	0.001003	4182	0.6
Water (100°C)	958.65	0.000282	4182	0.6791
Copper (20°C)	8978	-	381	387.6

https://doi.org/10.1017/pds.2023.59 Published online by Cambridge University Press

For the choice of the physical computational model, the Reynolds number (Re) is calculated for both fluids according to (4) due to different dynamic viscosities η. For this purpose, the hydraulic diameter (d_h) is calculated according to (3). As shown in Figure 2, if convergence is reached during the wall generation, areas of equal size are generated, resulting in the fluid cross-sectional area (A_{cs}) for the hot fluid (hf) and the cold fluid (cf) being equal and equal to 2.522e-4 m² (Figure 5). Therefore, the wetted perimeter (U_{cs}) of the cross-sectional area is 4.607e-1 m. Based on this information and the initial conditions that the velocity w at the inlet is 0.02 m/s and the defined density of water (Table 1), the Reynolds numbers are $Re_{hf} = 148.6$ and $Re_{cf} = 43.65$. Thus, laminar behavior occurs in both fluid flows, so a laminar computational model is used.

$$d_h = \frac{4 \cdot A_{cs}}{U_{cs}} \tag{3}$$

$$Re = \frac{w \cdot d_h \cdot \rho}{\eta} \tag{4}$$

2.2.2 Meshing

The meshing is performed with a top-down meshing workflow. First, a fine surface mesh is created. Due to the complexity of the generated structure (Figure 5), characterized by multi-radial curvatures and freeform surfaces, a curvature size function is defined, where the maximum angle of a mesh element to approximate a curvature is 3 degrees. Furthermore, a growth rate of 1.1 is defined for all volumes for an acceptable resolution. The boundary layers of the fluids are defined by the dimensionless wall distance of y+ ~ 1 for good results in heat transfer. In addition, 10 elements are defined as boundary layers with a load ratio of 0.2 for a slow change of the aspect ratio of the boundary layer starting from the first cell in the wall region. Due to the minimal wall spacing in some cases, a mesh of polyhedral cells is used as these elements are also well suited for heat transfer calculations (Baker, 2021). All further information is given in Table 2.

Table 2: Mesh parameter

Parameter	**Hot fluid volume**			**Cold fluid volume**			**Solid region**		
Y+	~1						-		
Growth rate	1.1						1.1		
Inflation Layers\ Boundary Layer	10						3		
Transition Ratio	0.2						0.3		
Max Cell Length	0.8								
Cell Type	polyhedral								
Mesh size									
Cell Size [mm]	Min.	Max.	Ave.	Min.	Max.	Ave.	Min.	Max.	Ave.
	8.8e-9	0.08	5.8e-5	1.1e-8	0.1	5.6e-5	2.5e-7	0.1	9.1e-5
Cells	47,848,524			49,433,840			50,364,107		
Quality	Min.	Max.	Ave.	Min.	Max.	Ave.	Min.	Max.	Ave.
Skewness	4.5e-7	0.8	**0.03**	2.4e-7	0.85	**0.03**	9.7e-8	0.8	**0.03**
Orthogonality	0.2	1	**0.97**	0.15	1	**0.97**	0.2	1	**0.97**
Aspect Ratio	1.3	85.7	**5.3**	1.3	173.7	**5.2**	1.3	50.7	**3.1**

The mesh quality was evaluated using three standard parameters: orthogonality, skewness, and aspect ratio. A minimum quality of 0.1 is defined for the orthogonality of the cells during mesh generation. From Table 2, it can be seen that the mesh is markedly better than 0.1 for all volumes. The worst orthogonality is in the mesh of the cold fluid. This can be attributed to problematic curvatures in the cross-section, which subsequently leads to isolated bad cells during mesh generation. However, all meshes show excellent cell quality concerning the average orthogonality and skewness. The aspect ratio varies greatly, but the average aspect ratio is at most 5.3, which is acceptable for polyhedral cell types.

https://doi.org/10.1017/pds.2023.59 Published online by Cambridge University Press

Furthermore, no problematic cells or cell clusters could be identified by optical cross-checking (Figure 6). The figure shows the section of the volume cells in the cross-section along the flow direction. Thus, the mesh represents the wall area very well.

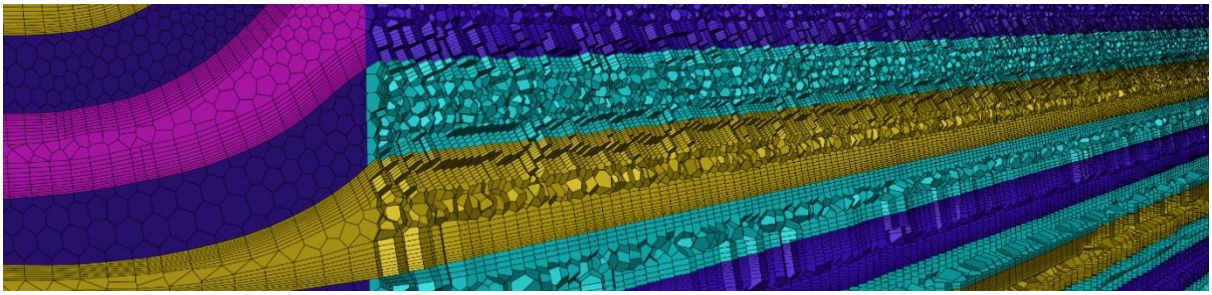

Figure 6. Section of the mesh plot with cells of the overall geometry

2.2.3 Simulation setup

A pressure-based solver with a pressure-velocity coupling method and the coupled algorithm is chosen for the calculation. For this algorithm, the momentum equation and the pressure-based continuity equation are solved together. A robust calculation of the fluids characterizes this coupled algorithm. The fluid behavior is calculated steady-state since the investigation focuses primarily on the geometry's thermal performance. (Baker, 2021)

Based on these solver settings, convergence criteria are defined for continuity at 1e-5 and energy at 1e-6. In addition to these quantities, the mass-weighted temperature ($\overline{\vartheta_x}$) (5) for cold fluid and hot fluid at the inlet and outlet and the mass-weighted pressure ($\overline{p_x}$) (6) and pressure drop (Δp) (11) is further tested for convergence. Besides, the log mean temperature difference ($\Delta\vartheta_M$) for parallel flow heat exchanger is calculated with (7). Subsequently, based on the temperature results, the heat flows ($\dot{Q}$) of the two fluids are calculated according to (9) under the condition of (8), using the heat flow of the cold fluid to determine the transferred or actual heat flow. The general heat transfer coefficient (U) is determined using (10). Finally, for an approximate efficiency evaluation of the heat exchanger's transferred heat output, the heat transfer efficiency (ε) is calculated using the modified ε-NTU-method (12) of Roopesh Tiwari (2017). This equation considers the achievable ideal temperature difference of parallel heat exchangers, which the classical ε-NTU-method does not give. All equations are based on the quantities $\dot{m}$ for the mass flow, A for the heat-transferring surface, ρ_x for the fluid density, and c_{px} for the fluid-specific heat capacity.

$$\overline{\vartheta_x} = \frac{\int \rho_x \cdot \vartheta_x dV}{\int \rho_x dV} \tag{5}$$

$$\overline{p_x} = \frac{\int \rho_x p_x dV}{\int \rho_x dV} \tag{6}$$

$$\Delta\vartheta_M = \frac{\left(\bar{\vartheta}_{hot_{in}} - \bar{\vartheta}_{cold_{in}}\right) - \left(\bar{\vartheta}_{hot_{out}} - \bar{\vartheta}_{cold_{out}}\right)}{\ln\left(\frac{\left(\bar{\vartheta}_{hot_{in}} - \bar{\vartheta}_{cold_{in}}\right)}{\left(\bar{\vartheta}_{hot_{out}} - \bar{\vartheta}_{cold_{out}}\right)}\right)} \tag{7}$$

$$\dot{Q}_1 \approx \dot{Q}_2 = \dot{Q} \tag{8}$$

$$\dot{Q}_x = \dot{m}_x \cdot c_{\mathrm{px}} \cdot \left(\left|\bar{\vartheta}_{x_{in}} - \bar{\vartheta}_{x_{out}}\right|\right) \tag{9}$$

$$U_x = \frac{min[\dot{Q}_x]}{A \cdot \Delta\vartheta_{M_x}} = \frac{\dot{Q}_{real}}{A \cdot \Delta\vartheta_{M_x}} \tag{10}$$

$$\Delta p = \bar{p}_{x_{in}} - \bar{p}_{x_{out}} \tag{11}$$

$$\varepsilon = \frac{\dot{Q}_{x_{min}}}{\dot{Q}_{ideal}} = \frac{\dot{m}_{min} \cdot c_p \cdot \min\left[\Delta\bar{\vartheta}_{hot}, \Delta\bar{\vartheta}_{cold}\right]}{U \cdot \mathrm{A} \cdot \mathrm{AMTD}} = \frac{\dot{m}_{min} \cdot c_{px} \cdot \left|\bar{\vartheta}_{\mathrm{min_{in}}} - \bar{\vartheta}_{\mathrm{min_{out}}}\right| \cdot 100\%}{U \cdot A \cdot 0.5 \cdot \left(\left(\bar{\vartheta}_{hot_{in}} + \bar{\vartheta}_{hot_{out}}\right) - \left(\bar{\vartheta}_{cold_{in}} + \bar{\vartheta}_{cold_{out}}\right)\right)} \tag{12}$$

https://doi.org/10.1017/pds.2023.59 Published online by Cambridge University Press

3 RESULTS

Due to the mesh size, the calculations were performed on the high-performance computing system (HPC) of TU Dresden. The results were calculated with the introduced formulas and are listed in Table 3. The calculation converged after 150 iterations. The temperature has cooled by 34.52 K for the hot fluid, and the cold fluid has heated up by 33.02 K. As a result, the pressure drop of the hot fluid (5.054 Pa) was lower due to the lower viscosity, while the pressure drop of the cold fluid (17.24 Pa) was correspondingly higher. Also, the resulting heat flux of the cold fluid is smaller than that of the hot fluid and is thus defined as the actual heat flux $\dot{Q}_{x_{min}}$ that was used to calculate the efficiency coefficient ε according to (12). The heat exchanger is thus characterized by a general heat transfer coefficient of 550.1 [W/ (m² K)]. The cooling behavior of the heat-transferring wall is shown in cross-section layer by layer along the Z-direction (Figure 7). The best heat transfer can be seen in the areas with many furrows, which is why the fluids cool fastest in the middle cross-sectional area. From the center, the cooling increases inhomogeneously towards the edge. In general, it can be seen that fluid regions partially or entirely enclosed by furrows cool faster. The velocity is smaller in the central region at smaller wall spacing because of the furrow sections than in the outer wall regions. As a result, the temperature drops more slowly in areas with larger mass flows due to an inhomogeneous mass flow distribution in the heat exchanger. The design presented in this study has an efficiency of 73.1% concerning the heat flow provided.

Table 3. Results of the numerical research on differential-growth heat exchanger

	Differential-growth heat exchanger		Gyroid-heat-exchanger (Peng *et al.*, 2019)	
Result values	Hot fluid	Cold fluid	Hot fluid	Cold fluid
$\bar{\vartheta}_{in}$ [K]	371.44	294.96	373.15	293.15
$\bar{\vartheta}_{out}$ [K]	336.92	327.68	335.43	330.95
$\Delta\vartheta_M$ [K]	31.47		26.23	
$\dot{m}$ [kg/s]	0.005		0.007	
$\dot{Q}$ [W]	726.8	695.2	1187.9	
U [W/($m^2 \cdot K$)]	550.1		1811.2	
Δp [Pa]	5.054	17.24	19.15	
$\dot{Q}_{ideal}$ [W]	950.6		1913.1	
ε [%]	73.1		62.1	

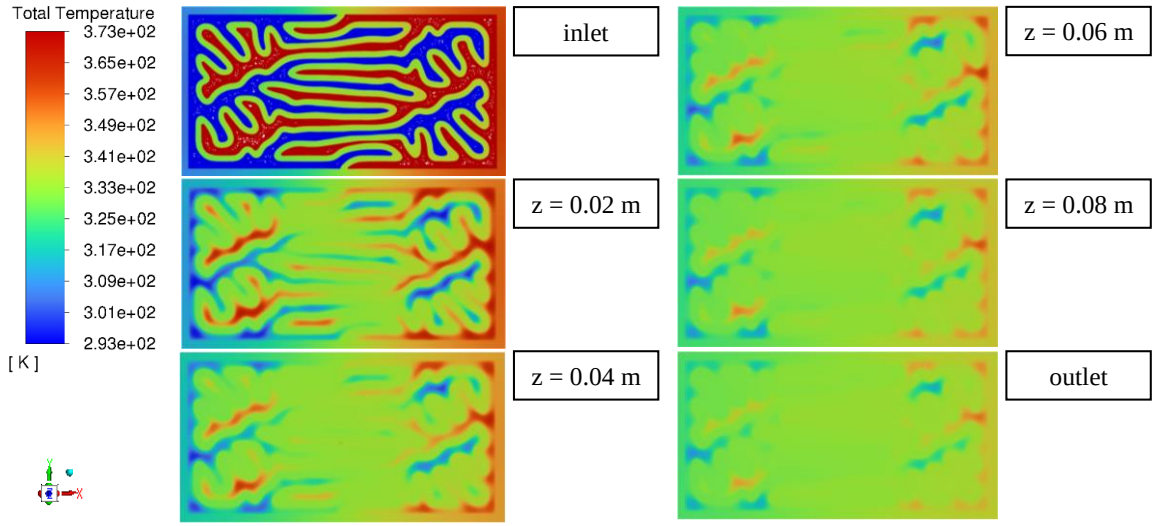

Figure 7. Evolution of the total temperature distribution of the cross-section in the Z-direction of the differential-growth heat exchanger

https://doi.org/10.1017/pds.2023.59 Published online by Cambridge University Press

The general heat transfer coefficient U, according to (10), was also determined for better comparability based on the study results (Peng *et al.*, 2019). The coefficient of heat transfer is 1811 W/ (m² K), which results in an ideal heat flux of 1913 W, according to (11). Based on (12), the heat flux efficiency of the gyro heat exchanger is 61.21%, with an actual heat flux of 1187.9 W. (Li et al., 2018)

4 DISCUSSION

Compared to the gyroid-heat exchanger by Peng et al. (2019), the presented method generated a heat exchanger with a 37.76% larger heat-transferring wall. In addition, this method can also generate a geometry with significantly higher surface areas than TPMS structures. However, by choosing the same design space, the flow-through area of the heat exchanger was reduced by approximately 31.04%, compared to the gyroid-heat exchanger, due to the larger surface area of the wall and the larger wall thickness due to manufacturing constraints. However, the maximum pressure drop in the heat exchanger presented here is smaller by 10%. This is due, among other things, to the fact that such structures have a more homogeneous flow pattern. In contrast, TPMS structures create turbulence flow pattern in the fluid despite laminar flows due to the channel-like structures with complex curved surfaces. This leads to better mixing of the fluids, which positively affects energy transfer, as seen in Table 3. However, the efficiency factor calculated according to (12) shows that the structure presented in this study can realize the maximum achievable heat flux much better with 73.1% than the heat exchanger (Peng *et al.*, 2019). This can be attributed to the geometry characteristics of the structure, as the different furrows allow the heat transfer to be explicitly controlled in the fluid. As a result, these structures can react more flexibly to different thermal conditions in the fluids.

5 CONCLUSION

In this study, a heat-transferring wall for heat exchangers generated by the differential-growth method was investigated for the first time, to the author's knowledge, in terms of its thermal and fluid-mechanical properties to assess the potential of the geometry-generating method. Compared to TPMS-approximated wall structures, the investigated wall structure has a significantly higher realized heat transfer than the ideal possible heat transfer. Furthermore, it has been observed that with this structure, the heat transfer in pure laminar flow is closer to the ideal achievable heat transfer than in gyroid-heat exchangers. Furthermore, it has been shown that the furrow design positively affects the heat transfer rate. This has revealed a further potential for this method of designing heat-transferring walls. Thus, it is conceivable to realize targeted cooling processes via the furrow design's characteristics and distribution over the cross-section. Due to these potentials and the lower pressure losses, the possibilities of the differential-growth method could be shown in this investigation.
Furthermore, this investigation showed a new promising approach for generating complex wall structures for heat exchangers, which should be investigated in more detail. In this context, additional parameters or field functions for a functionally targeted control of the growth behavior require further definitions. Likewise, the inflow and outflow area should be considered in future investigations to include a more realistic representation of the flow characteristics of the heat exchanger. For the numerical investigation, the next step should be to optimize the mesh to ensure a faster calculation, shorter feedback loops, and a more realistic representation of flow patterns with experimentally validated results. Furthermore, alternative calculation methods, such as the Lattice-Boltzmann method for the design of such complex geometries, should be analyzed.

ACKNOWLEDGMENTS

The authors thank the Center for Information Services and High-Performance Computing [Zentrum für Informationsdienste und Hochleistungsrechnen (ZIH)] at TU Dresden for providing its facilities for high throughput calculations.

REFERENCES

Attarzadeh, R., Rovira, M. and Duwig, C. (2021), “Design analysis of the “Schwartz D” based heat exchanger: A numerical study”, *International Journal of Heat and Mass Transfer*, Vol. 177, p. 121415. https://dx.doi.org/10.1016/j.ijheatmasstransfer.2021.121415

https://doi.org/10.1017/pds.2023.59 Published online by Cambridge University Press

Attarzadeh, R., Attarzadeh-Niaki, S.-H. and Duwig, C. (2022), "Multi-objective optimization of TPMS-based heat exchangers for low-temperature waste heat recovery", Applied Thermal Engineering, Vol. 212, p. 118448. https://dx.doi.org/10.1016/j.applthermaleng.2022.118448

Baker, T.J. (2021), "Ansys Fluent User's Guide 2021 R2", *User Guids*, ANSYS, Inc.

Genç, A.M., Vatansever, C., Koçak, M. and Karadeniz, Z.H. (2022), "Investigation of additively manufactured triply periodic minimal surfaces as an air-to-air heat exchanger", CLIMA 2022 conference, 2022: CLIMA 2022 The 14th REHVA HVAC World Congress. https://dx.doi.org/10.34641/clima.2022.172

Gotsman, C. and Lindenbaum, M. (1996), "On the metric properties of discrete space-filling curves", *IEEE transactions on image processing a publication of the IEEE Signal Processing Society*, Vol. 5 No. 5, pp. 794–797. https://dx.doi.org/10.1109/83.499920

Jafari, D. and Wits, W.W. (2018), "The utilization of selective laser melting technology on heat transfer devices for thermal energy conversion applications: A review", *Renewable and Sustainable Energy Reviews*, Vol. 91, pp. 420–442. https://dx.doi.org/10.1016/j.rser.2018.03.109

Li, W., Yu, G. and Yu, Z. (2020), "Bioinspired heat exchangers based on triply periodic minimal surfaces for supercritical CO2 cycles", *Applied Thermal Engineering*, Vol. 179, p. 115686. https://dx.doi.org/10.1016/j.applthermaleng.2020.115686

Pedersen, H. and Singh, K. (2006), "Organic labyrinths and mazes", in DeCarlo, D. and Markosian, L. (Eds.), *Proceedings of the 3rd international symposium on Non-photorealistic animation and rendering - NPAR '06, 05.06.2006 - 07.06.2006, Annecy, France*, ACM Press, New York, New York, USA, p. 79. https://dx.doi.org/10.1145/1124728.1124742

Peng, H., Gao, F. and Hu, W. (2019), *Design, Modeling and Characterization on Triply Periodic Minimal Surface Heat Exchangers with Additive Manufacturing*, University of Texas at Austin.

Roopesh Tiwari, D.M. (2017), "Effectiveness and Efficiency Analysis of Parallel Flow and Counter Flow Heat Exchangers", *International Journal of Application or Innovation in Engineering & Management (IJAIEM)*, pp. 314–319.

Shah, R.K., Thonon, B. and Benforado, D.M. (2000), "Opportunities for heat exchanger applications in environmental systems", *Applied Thermal Engineering*, Vol. 20 No. 7, pp. 631–650. https://dx.doi.org/10.26153/tsw/17483

Vlahinos, M. and O'Hara, R. (2020), "Unlocking Advanced Heat Exchanger Design and Simulation with nTop Platform and ANSYS CFX". *nTopology*

Zhu, Z., Li, J., Peng, H. and Liu, D. (2021), "Nature-Inspired Structures Applied in Heat Transfer Enhancement and Drag Reduction", *Micromachines*, Vol. 12 No. 6. https://dx.doi.org/10.3390/mi12060656

https://doi.org/10.1017/pds.2023.59 Published online by Cambridge University Press